High spatial resolution correlated investigation of Zn segregation to stacking faults in ZnTe/CdSe nanostructures

Bastien Bonef, Adeline Grenier, Lionel Gérard, Pierre-Henri Jouneau, Régis André, Didier Blavette, Catherine Bougerol

High spatial resolution correlated investigation of Zn segregation to stacking faults in ZnTe/CdSe nanostructures

Bastien Bonef, Adeline Grenier, Lionel Gerard, Pierre-Henri Jouneau, Regis André, Didier Blavette, and Catherine Bougerol

Citation: Appl. Phys. Lett. **112**, 093102 (2018); doi: 10.1063/1.5020440
View online: https://doi.org/10.1063/1.5020440
View Table of Contents: http://aip.scitation.org/toc/apl/112/9
Published by the American Institute of Physics

High spatial resolution correlated investigation of Zn segregation to stacking faults in ZnTe/CdSe nanostructures

Bastien Bonef,[1] Adeline Grenier,[2] Lionel Gerard,[3] Pierre-Henri Jouneau,[1] Regis André,[3] Didier Blavette,[4] and Catherine Bougerol[3]
[1]*Université Grenoble Alpes, CEA, INAC, F-38000 Grenoble, France*
[2]*CEA-LETI, F-38054 Grenoble, France*
[3]*Université Grenoble Alpes, CNRS, Institut Néel, F-38000 Grenoble, France*
[4]*Normandy University, Groupe de Physique des Matériaux, INSA ROUEN, CNRS, 76000 Rouen, France*

(Received 22 December 2017; accepted 9 February 2018; published online 26 February 2018)

The correlative use of atom probe tomography (APT) and energy dispersive x-ray spectroscopy in scanning transmission electron microscopy (STEM) allows us to characterize the structure of ZnTe/CdSe superlattices at the nanometre scale. Both techniques reveal the segregation of zinc along [111] stacking faults in CdSe layers, which is interpreted as a manifestation of the Suzuki effect. Quantitative measurements reveal a zinc enrichment around 9 at. % correlated with a depletion of cadmium in the stacking faults. Raw concentration data were corrected so as to account for the limited spatial resolution of both STEM and APT techniques. A simple calculation reveals that the stacking faults are almost saturated in Zn atoms (∼66 at. % of Zn) at the expense of Cd that is depleted. *Published by AIP Publishing*. https://doi.org/10.1063/1.5020440

Recent studies reported the possibility of using ZnTe/CdSe based superlattices (SLs) as promising candidates for photovoltaic devices.[1,2] First, the type-II band alignment between ZnTe and CdSe enables the direct spatial separation of the photogenerated carriers.[3] Also, the absorption of the SLs can be tuned to match the visible spectrum by varying the layer thicknesses and the number of periods.[4] The typical limitation for the growth of long period SLs is the accumulation of strain which ultimately places limits on the active layer thickness. Since ZnTe and CdSe are nearly lattice matched semiconductors ($a = 0.6103$ nm and 0.6078 nm, respectively), almost strain free SLs can be grown. However, one of the limitations of growing such solar cells then arises from the necessity to find substrates which are cost-effective. Since ZnTe substrates are expensive and complicated to produce, foreign substrates are required. GaAs is proposed as an alternative substrate to ZnTe. However, the large lattice mismatch between the two semiconductors (7.9%) is responsible for the relaxation of the epitaxially grown ZnTe and the formation of structural defects such as stacking faults. These defects have been extensively imaged using atomic scale characterization techniques such as transmission electron microscopy. However, local chemical composition modifications near the defect line remain challenging to evidence and require the use of chemically sensitive nanometre scale characterization techniques.

Energy dispersive x-ray spectroscopy (EDX) in scanning transmission electron microscopy (STEM) and atom probe tomography (APT) were combined to investigate the local chemistry of stacking faults (SFs) in ZnTe/CdSe SLs grown on GaAs by molecular beam epitaxy (MBE). APT is a powerful technique which provides composition information with a nanometre resolution.[5,6] It has now been extensively applied for the investigation of interfaces or defects in II-VI semiconductors.[7–13] However, strict atomic resolution cannot be achieved on such materials, and more importantly, calibration of the APT evaporation parameters is required to get reliable quantifications.[8,12–17] The correlative use of APT with EDX measurements allows the overcoming of these limitations. Such an approach has been successfully applied for the structural characterization of other II-VI and III-nitride semiconductors.[18–22] In this study, both APT and EDX were able to evidence the segregation of zinc along SFs. Both spatial limitations of the techniques are discussed to explain the observed Zn distribution, and a simple model is proposed to extract the real Zn enrichment along the faults.

The super-lattice is composed of 10 periods of 50 nm CdSe and 20 nm ZnTe grown on a GaAs (001) substrate by molecular beam epitaxy (MBE). The two binary compounds were grown following standard conditions at a growth temperature of 340 °C. ZnTe was grown under Zn excess,[23,24] while CdSe under Se excess.[25] A 150 nm thick ZnTe buffer layer was grown between the substrate and the super-lattice to lower the strain and reduce the propagation of structural defects to the active region. The super-lattice was grown with a growth rate of around 0.75 monolayer (ML) per second (1 ML = 0.305 nm). The total time of the growth for the super-lattice is around 50 min. Needle shaped specimens are required to promote field evaporation in atom probe analyses.[5] Atom probe tips were shaped on a FEI Strata 400S and were prepared so that the direction of APT analysis was parallel to the [00–1] direction (top down-analyses).[26] To avoid damage to the material during FIB preparation, the acceleration voltage of the Ga ions was progressively decreased from 30 keV to 5 keV during the process. A final cleaning of the tips at 2 keV was used to lower irradiation damage. The specimen imaged using STEM was also prepared using the standard lift-out technique and heterogeneously thinned down during the last milling to obtain a final thickness ranging from 150 nm to 50 nm. A thin enough region for the transmission of electrons with few defects and contamination deposits was chosen to image the super-lattice. This was

performed in the bright-field STEM mode on a FEI Tecnai Osiris microscope operated at 200 keV and equipped with a field electron gun source. Observations were made along a [110] zone axis. Chemical analyses were performed by EDX. The four silicon drift detector (SDD) set on the microscope provided a collection angle for X-rays of 0.9 sr. This enables the formation of chemical maps in less than 10 min, and the exposition of the sample to the electron beam is then minimized. The APT investigations were performed using a CAMECA Flextap equipped with an amplified infra-red laser providing a pulse duration of 450 fs, a spot size of 10 μm, and a repetition rate of 100 kHz. The top-down geometry for the tip analysis (the first layer grown is the last to be evaporated) was chosen to have the interfaces between the ZnTe/CdSe oriented perpendicular to the evaporation direction. The specificity of the Flextap lies in the possibility of tuning the path of the ions in the chamber. The flexible optics set around the chamber provide variable fields of view (up to 165 nm diameter) or a high mass resolution (up to m/Δ3000). The studies carried on ZnTe and CdSe required a configuration where the mass resolution is enhanced at the expense of the field of view to resolve the different isotopes of Zn, Cd, Se, and Te, and consequently, the accuracy of the quantification is increased. The evaporation of the superlattice was performed under green exposure and at 2 nJ. The tip was cooled down to 20 K to optimize the spatial resolution,[27] and the detection rate was set at 0.005 ions.pulse^{-1}. The 3D reconstruction of the volume was optimized using SEM images of the tip and by adjusting the initial tip radius and the detection efficiency of the instrument so as to obtain flat interfaces between CdSe and ZnTe as well as the correct thicknesses of the layers measured from TEM (Fig. 1).[28]

Figure 1 shows a bright field TEM image of 3 ZnTe/CdSe periods where the interfaces between the different layers can be clearly identified. The average thicknesses of the ZnTe and CdSe layers are 21 nm and 48 nm, respectively. Patches of darker contrast can be observed mostly in CdSe layers. These are certainly caused by the preparation of the specimen by FIB. In Fig. 1, a high density of [111] SFs can be observed. The observed stacking faults originate from the relaxation of the ZnTe/CdSe layers in spite of the presence of the ZnTe buffer layer.

Figure 2(a) presents the EDX chemical map of Zn obtained on a period of the SL shown in the STEM-HAADF image in Fig. 2(b). It can be seen that besides the ZnTe layer, Zn is also visible in the CdSe ones. The Zn signal in the CdSe layers correspond to the [111] SF evidenced in Fig. 2(b). EDX chemical distributions were also extracted for Cd, Se, and Te, and no enrichments in these elements along SFs were detected. From the EDX maps, quantitative profiles of Zn, Cd, Se, and Te were obtained across the SFs [Fig. 2(c)]. The Cliff-Lorimer method was used to convert the X-ray intensities of the different elements into atomic concentrations.[29] The lateral size of the sampling volume is 20 nm to increase the signal to noise ratio. The accuracy of the Cliff-Lorimer quantification (k-factor) was verified by measuring the calculated composition ratios between II and VI elements. Here, the average (Zn + Cd)/(Te + Se) ratio is 1.05, which is in very good agreement with the expected 1:1 ratio. This consequently validates the k-factor quantification

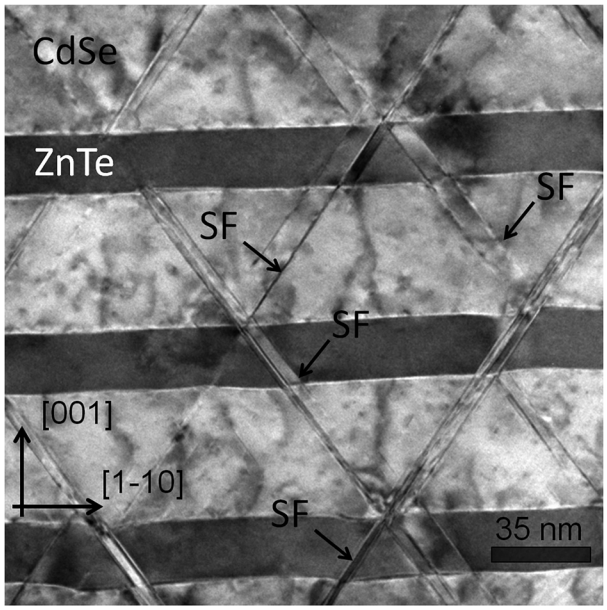

FIG. 1. Bright field TEM image of the ZnTe/CdSe superlattice showing the different layers and the presence of [111] stacking faults.

method. The presence of Zn in the SFs can be clearly evidenced in the profile with the increase in the Zn concentration from 1% in the CdSe layer up to 5.5% in the fault. It is however difficult to confirm that the increase in the Zn signal corresponds to the decrease in the other type II element Cd, with statistical fluctuations being in the order of 5% in the case of Cd and Se. Moreover, the full width at half maximum of the Zn distribution is 6 nm which is more than 7 times the width of a SF. The spatial resolution in EDX is limited by the probe broadening effect.[19] Because of the FIB preparation, the thickness of the TEM specimen is expected to be above 100 nm, resulting in a probe size being larger than the width of the SF. Consequently, the quantification in the SF is affected by the surrounding CdSe matrix, leading to not only an under-estimation of the Zn composition but also to the artificial observation of Zn on the side of the fault. Also, if the SF (planar defect) is not perfectly oriented parallel to the beam direction, then it will result in such broadening of the Zn distribution. However, this could also be material related

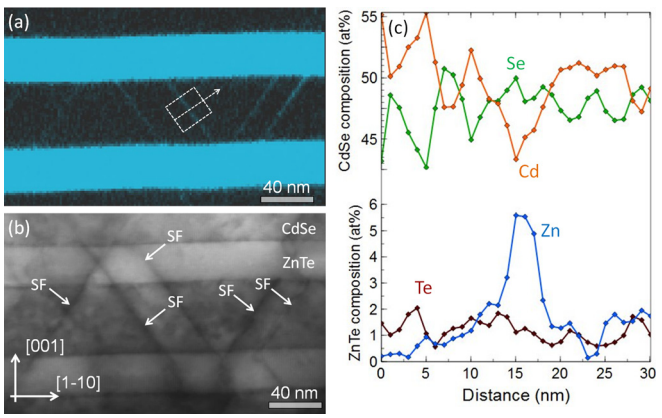

FIG. 2. (a) Zn distribution obtained from EDX corresponding to the image in (b). (b) STEM-HAADF image of one period of the superlattice showing the presence of stacking faults. (c) 1 D concentration profile corresponding to the sampling area shown in (a) and measured perpendicular to the fault.

and Zn could be present not only along the SF but also in the surrounding CdSe. The broadening of the electron beam along the thickness of the TEM lamella is an intrinsic limitation of the technique. In this study, the APT 3D reconstruction ability compensates for the projection limitation of transmission electron microscopy.

Figures 3(a) and 3(b) show the 3D distribution of Cd, Se, Zn, and Te atoms in 4 periods of the superlattice obtained from APT. Away from SFs, Zn is not detected in the CdSe layer. Figure 3(b) shows the same 3D distribution showing only Zn atoms. Despite the small sampling volume of APT analysis compared to the large field of view of TEM, the large number of SFs in the sample allows for the direct visualization of two faults in this APT reconstruction. Again, no enrichment in Cd, Se, and Te along SFs is observed. A small volume ($11 \times 11 \times 17\,\text{nm}^3$) was extracted perpendicular to the fault in Fig. 3(b) and is shown in Fig. 3(c). A uniform distribution of Zn along the fault is observed and was confirmed by drawing a 1D concentration profile along the fault. The distribution of Zn appears to be around 6 nm wide, and the Zn atoms observed away from the fault and in the CdSe layer are attributed to noise counts. Figure 3(d) shows the corresponding 1D concentration profile of Zn, Cd, and Se measured perpendicular to the SF with a sampling step of 0.2 nm. This concentration profile reveals that the increase in the Zn signal is correlated with a decrease in the Cd signal that is of the same amplitude (~8%). Consequently, Zn atoms are most likely to be in substitution of Cd atoms in the crystal structure. The Zn peak is enlarged (w = 6 nm) and much larger than the actual width of SFs (~ d_{111}). This is due to the spatial resolution of APT that is limited by local trajectory aberrations that affect the ion trajectory close to SFs. Such aberrations are caused by local magnification effects due to differences in tip curvatures related to the presence of regions of different evaporation fields.[30,31] Here, the presence of ZnSe bonds in the fault which have a larger cohesive energy (2.69 eV) compared to CdSe (2.52 eV) could lead to CdZnSe being more difficult to evaporate compared to CdSe.[32] This would be responsible for the formation of a protuberance on the tip surface during the evaporation of the fault. This leads to the well-known defocusing effects that may give rise to trajectory overlaps and biased composition levels. The ions leaving the protuberance would be projected away from it and consequently would overlap the trajectories of the surrounding ions originating from the CdSe matrix.[33,34] The observed peak atomic fraction of Zn in SFs [around 9 at. % in Fig. 3(d)] is therefore underestimated. A correction may be brought about, which is based on the conservation of the amount of solute elements in the segregated region. The integral of the concentration profile, which is proportional to the total number of solute atoms segregated to the defect, is not affected by trajectory overlaps. Assuming that the concentration peak [Fig. 3(d)] has a Gaussian shape (width $w \sim 4\sigma$, with σ being the standard deviation of the Gaussian distribution), a simple calculation shows that the real concentration C* can be derived from the peak measured concentration C as follows:

$$C^* = C\frac{\sigma\sqrt{2\pi}}{\delta},$$

where δ is the actual width of the [111] SF ($d_{111} = 0.5$ nm) and $\sigma = w/4$ is equal to 1.5 nm according to Fig. 3(d). This correction is based on the transformation of the experimental Gaussian profile into a square wave of height C* and width δ. It leads to a concentration of 66 at. % in the SF. The defect is then highly concentrated in Zn atoms (ideally 100% of Zn). The same correction was applied to the EDX profile [Fig. 2(c)] and leads to a similar value of 60 at. %. A practical way to investigate the actual Zn distribution in the SFs would be to align some defects parallel to the tip surface in order to take advantage of the improved spatial resolution of the atom probe along the evaporation direction (perpendicular to the tip surface).[5] The experiment would require the preparation of an APT sample oriented 60° relative to the [001] direction. Similar preparation involving the rotation of the samples 180° relative to the growth direction has already been successfully performed with a FIB.[35,36]

This Zn segregation to SFs in CdSe layers may be interpreted as a Suzuki effect.[37] The segregation of solute elements to crystal defects is known to decrease the energy of defects and may stabilize them. This is theoretically predicted and experimentally observed in both grain boundaries[38] which can

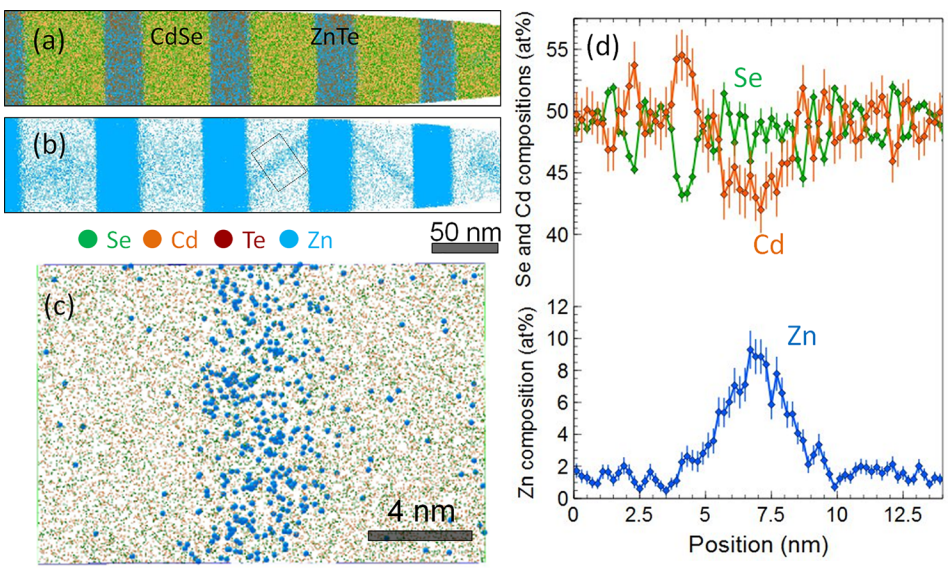

FIG. 3. (a) and (b) 3D APT reconstruction of the superlattice showing the distribution of Zn, Te, Cd, and Se atoms. (c) Zoom of the Zn distribution along the fault displayed in (b). Evolution of Zn, Cd, and Se taken from the sampling volume in (c) and across the stacking fault.

be reinforced by the segregation of impurities (boron in nickel base super-alloys[39]), dislocations (Cottrell atmospheres in FeAl inter-metallics[40]), and antiphase boundaries as well as SFs.[41,42] In FeAl inter-metallics, boron segregation to SFs is even thought to be responsible for the stabilization of [001] SFs that are known to be of high energy in BCC structures. In the present case, Zn segregation at the expense of Cd [Fig. 3(d)] could stabilize these [111] SFs. The apparent amplitude of the segregation peak [Fig. 3(d)] is around 8 at. %, a value that is close to the concomitant drop of the atomic fraction of Cd in the central region of the SF. It is worth mentioning that SFs are observed to entirely cross CdSe and ZnTe layers (Fig. 1). It is therefore thought that it is not bulk diffusion of Zn in CdSe that controls the segregation kinetics but instead the migration of Zn from ZnTe layers along SFs.

In conclusion, nanometre scale structural and chemical information on ZnTe/CdSe superlattices has been obtained through the correlative use of STEM-EDX and APT. Both techniques highlight the segregation of Zn along [111] stacking faults observed across the entire superlattice in the CdSe layers. This Zn enrichment corresponds to a depletion of Cd and is interpreted as a Suzuki effect.[37] Since the spatial resolutions of EDX and APT are limited by the probe broadening effect and local magnification artifacts, respectively, the Zn distribution observed perpendicular to the stacking faults appears wider than in reality. A simple calculation reveals that defects are actually highly elevated with Zn atoms (66 at. %). The presence of [111] stacking faults could be avoided when growth of the superlattices is performed on the ZnTe substrate.[7,8] Since structural defects are known to act as traps for the carriers, growth of ZnTe/CdSe based photovoltaic devices should be performed on such substrates. The improvement in the crystal quality of the active region should result in an improvement of the optical properties of the device.

[1]R. André, E. Bellet-Amalric, J. Bleuse, C. Bougerol, S. Boyer-Richard, L. Gérard, H. Mariette, and J.-P. Richters, in *17th European Molecular Beam Epitaxy Workshop* (2013).
[2]S. Boyer-Richard, C. Robert, L. Gérard, J.-P. Richters, R. André, J. Bleuse, H. Mariette, J. Even, and J. M. Jancu, in *ICSNN Proceeding* (2012), p. 1.
[3]C. G. Van De Walle, Phys. B: Condens. Matter **376–377**, 1–6 (2006).
[4]S. Boyer-Richard, C. Robert, L. Gérard, J.-P. Richters, R. André, J. Bleuse, H. Mariette, J. Even, and J.-M. Jancu, Nanoscale Res. Lett. **7**, 543 (2012).
[5]D. J. Larson, T. J. Prosa, R. M. Ulfig, B. P. Geiser, and T. F. Kelly, *Local Electrode Atom Probe Tomography* (Springer, 2013).
[6]B. Gault, F. Vurpillot, A. Vella, M. Gilbert, A. Menand, D. Blavette, and B. Deconihou, Rev. Sci. Instrum. **77**, 043705 (2006).
[7]B. Bonef, B. Haas, J.-L. Rouvière, R. André, C. Bougerol, A. Grenier, P.-H. Jouneau, and J.-M. Zuo, J. Microsc. **262**, 178 (2016).
[8]B. Bonef, L. Gérard, J.-L. Rouvière, A. Grenier, P.-H. Jouneau, E. Bellet-Amalric, H. Mariette, R. André, and C. Bougerol, Appl. Phys. Lett. **106**, 051904 (2015).
[9]H. Benallali, T. Cremel, K. Hoummada, D. Mangelinck, R. André, S. Tatarenko, and K. Kheng, Appl. Phys. Lett. **105**, 053103 (2014).
[10]H. Benallali, K. Hoummada, M. Descoins, P. Rueda-Fonseca, L. Gerard, E. Bellet-Amalric, S. Tatarenko, K. Kheng, and D. Mangelinck, Scr. Mater. **69**, 505 (2013).
[11]D. J. Larson, D. A. Reinhard, T. J. Prosa, D. Olson, D. Lawrence, P. H. Clifton, R. M. Ulfig, T. F. Kelly, and V. S. Smentkowski, Microsc. Microanal. **18**, 928 (2012).
[12]E. Di Russo, L. Mancini, F. Moyon, S. Moldovan, J. Houard, F. H. Julien, M. Tchernycheva, J. M. Chauveau, M. Hugues, G. Da Costa, I. Blum, W. Lefebvre, D. Blavette, and L. Rigutti, Appl. Phys. Lett. **111**, 032108 (2017).
[13]L. Rigutti, L. Mancini, E. Di Russo, I. Blum, F. Moyon, W. Lefebvre, D. Blavette, F. Vurpillot, E. Giraud, J. F. Carlin, R. Butté, N. Grandjean, N. Gogneau, L. Largeau, F. H. Julien, M. Tchernycheva, J. M. Chauveau, M. Hugues, R. Agrawal, R. A. Bernal, D. Isheim, H. D. Espinosa, J. R. Riley, R. A. Bernal, Q. Li, H. D. Espinosa, G. T. Wang, L. J. Lauhon, A. Devaraj, R. Colby, W. P. Hess, D. E. Perea, S. Thevuthasan, D. R. Diercks, B. P. Gorman, R. Kirchhofer, N. Sanford, K. Bertness, M. Brubaker, L. Mancini, N. Amirifar, D. Shinde, I. Blum, M. Gilbert, A. Vella, F. Vurpillot, W. Lefebvre, R. Lardé, E. Talbot, P. Pareige, X. Portier, A. Ziani, C. Davesnne, C. Durand, J. Eymery, R. Butté, J.-F. Carlin, N. Grandjean, L. Rigutti, N. Amirifar, R. Lardé, E. Talbot, P. Pareige, L. Rigutti, L. Mancini, J. Houard, C. Castro, V. Sallet, E. Zehani, S. Hassani, C. Sartel, A. Ziani, X. Portier, and D. R. Kingham, Microsc. Microanal. **22**, 650 (2016).
[14]M. Müller, G. D. W. Smith, B. Gault, and C. R. M. Grovenor, J. Appl. Phys. **111**, 064908 (2012).
[15]B. Bonef, R. Cramer, and J. S. Speck, J. Appl. Phys. **121**, 225701 (2017).
[16]L. Rigutti, L. Mancini, W. Lefebvre, J. Houard, D. Hernàndez-Maldonado, E. Di Russo, E. Giraud, R. Butté, J.-F. Carlin, N. Grandjean, D. Blavette, and F. Vurpillot, Semicond. Sci. Technol. **31**, 095009 (2016).
[17]L. Rigutti, L. Mancini, D. Hernández-Maldonado, W. Lefebvre, E. Giraud, R. Butté, J. F. Carlin, N. Grandjean, D. Blavette, and F. Vurpillot, J. Appl. Phys. **119**, 105704 (2016).
[18]B. Bonef, H. Boukari, A. Grenier, I. Mouton, P.-H. Jouneau, H. Kinjo, and S. Kuroda, Microsc. Microanal. **23**, 717–723 (2017).
[19]B. Bonef, M. Lopez-Haro, L. Amichi, M. Beeler, A. Grenier, E. Robin, P.-H. Jouneau, N. Mollard, I. Mouton, E. Monroy, and C. Bougerol, Nanoscale Res. Lett. **11**, 461 (2016).
[20]B. Bonef, M. Catalano, C. Lund, S. P. Denbaars, S. Nakamura, U. K. Mishra, M. J. Kim, and S. Keller, Appl. Phys. Lett. **110**, 143101 (2017).
[21]F. F. Krause, J.-P. Ahl, D. Tytko, P.-P. Choi, R. Egoavil, M. Schowalter, T. Mehrtens, K. Müller-Caspary, J. Verbeeck, D. Raabe, J. Hertkorn, K. Engl, and A. Rosenauer, Ultramicroscopy **156**, 29 (2015).
[22]M. Catalano, B. Bonef, C. Lund, U. K. Mishra, S. Keller, and M. J. Kim, Microsc. Microanal. **23**, 1448 (2017).
[23]R. D. Feldman, R. F. Austin, P. M. Bridenbaugh, A. M. Johnson, W. M. Simpson, B. A. Wilson, and C. E. Bonner, J. Appl. Phys. **64**, 1191 (1988).
[24]S. Tatarenko, B. Daudin, and D. Brun-Le Cunff, Appl. Phys. Lett. **66**, 1773 (1995).
[25]H. Luo, N. Samarth, F. C. Zhang, A. Pareek, M. Dobrowolska, J. K. Furdyna, K. Mahalingam, N. Otsuka, W. C. Chou, A. Petrou, and S. B. Qadri, Appl. Phys. Lett. **58**, 1783 (1991).
[26]K. Thompson, D. Lawrence, D. J. Larson, J. D. Olson, T. F. Kelly, and B. Gorman, Ultramicroscopy **107**, 131 (2007).
[27]B. Gault, M. Müller, A. La Fontaine, M. P. Moody, A. Shariq, A. Cerezo, S. P. Ringer, and G. D. W. Smith, J. Appl. Phys. **108**, 044904 (2010).
[28]F. Vurpillot, B. Gault, B. P. Geiser, and D. J. Larson, Ultramicroscopy **132**, 19 (2013).
[29]G. Cliff and G. W. Lorimer, J. Microsc. **103**, 203 (1975).
[30]F. Vurpillot, D. Larson, and A. Cerezo, Surf. Interface Anal. **36**, 552 (2004).
[31]N. Rolland, F. Vurpillot, S. Duguay, B. Mazumder, J. S. Speck, and D. Blavette, Microsc. Microanal. **23**, 247 (2017).
[32]X. W. Zhou, D. K. Ward, J. E. Martin, F. B. van Swol, J. L. Cruz-Campa, and D. Zubia, Phys. Rev. B **88**, 085309 (2013).
[33]F. Vurpillot, A. Bostel, and D. Blavette, Appl. Phys. Lett. **76**, 3127 (2000).
[34]D. Blavette, F. Vurpillot, P. Pareige, and A. Menand, Ultramicroscopy **89**, 145 (2001).
[35]D. J. Larson, T. J. Prosa, B. P. Geiser, and W. F. Egelhoff, Ultramicroscopy **111**, 506 (2011).
[36]T. Prosa, D. Lawrence, D. Olson, D. Larson, and E. Marquis, Microsc. Microanal. **15**, 298 (2009).
[37]H. Suzuki, J. Phys. Soc. Jpn. **17**, 322 (1962).
[38]D. Mc Lean, *Grain Boundaries in Metals* (Clarendon press, Oxford, 1956), Chap. 5.
[39]D. Lemarchand, E. Cadel, S. Chambreland, and D. Blavette, Philos. Mag. A **82**, 1651 (2002).
[40]D. Blavette, E. Cadel, A. Fraczkiewicz, and A. Menand, Science **286**, 2317–2319 (1999).
[41]E. Cadel, A. Fraczkiewicz, and D. Blavette, Scr. Mater. **51**, 437 (2004).
[42]E. Cadel, A. Fraczkiewicz, and D. Blavette, Annu. Rev. Mater. Sci. **33**, 215 (2003).